J Vis
https://doi.org/10.1007/s12650-019-00567-4

SHORT PAPER

Linyue Gao · Ramsankar Veerakumar · Yang Liu · Hui Hu

Quantification of the 3D shapes of the ice structures accreted on a wind turbine airfoil model

Received: 26 February 2019 / Revised: 7 May 2019 / Accepted: 9 May 2019

1 Introduction

Wind turbine icing has been found to cause a variety of problems to the safety and efficient operations of wind turbines in cold weather. Ice accretion on turbine blades could significantly alter the aerodynamic shape of turbine blades and increase surface roughness, resulting in severe power losses, load imbalances and excessive vibrations (Dalili et al. 2009). Ice accretion has also been found to cause structural failures of wind turbines, especially when coupled with strong wind loads (Battisti 2015). Wind turbine icing can also directly impact personnel safety due to the falling and projected large ice chunks (Morgan et al. 1998). It should be noted that icing hazard is often more severe in the locations which are best suited for wind turbine sites, such as northern latitudes, offshore wind farms and high altitudes (i.e., mountains), where wind turbines are more prone to water contamination and icing in cold weather.

While several studies have been carried out recently to investigate effects of ice accretion on wind turbine blades through icing wind tunnel testing (Hochart et al. 2008; Li et al. 2014; Yin et al. 2016) or using ''artificial'' iced profiles with various types and amounts of ice accretion to investigate the aerodynamic performance and power output for iced blades (Tammelin et al. 1999), very few icing physics studies can be found in the literature to elucidate the underlying physics pertinent to wind turbine icing phenomena. Although a number of anti-/de-icing systems have been used for wind turbine icing mitigation, almost all the current turbine icing protection strategies were originally developed for aircraft anti-/de-icing applications. Many special issues related to wind turbine icing phenomena have not been fully understood in adopting those aircraft-orientated anti-/de-icing techniques for wind turbine icing mitigation. For example, the optimized airfoil shapes of wind turbine blades usually have much greater airfoil thickness and blunter leading edge, in comparison with those used to design aircraft wings. The significant differences in the airfoil shapes, especially in the regions near the airfoil leading edges, would greatly affect the flying trajectories of the supercooled water droplets carried by the incoming airflow, thereby, the subsequent droplet impinging dynamics and water collection characteristics over the airfoil surface, resulting in significant changes in the ice accretion characteristics and topologies of the ice structures accreted over the turbine blade surface.

In the present study, an experimental investigation was conducted to characterize the dynamic ice accreting process over the surfaces of a typical wind turbine blade model. The experimental study was performed in an Icing Research Tunnel available at Iowa State University (i.e., ISU-IRT). A composite-based turbine blade section model with the most commonly used DU91-W2-250 airfoil profile in the cross section was designed and manufactured for the ice accretion experiments under a typical glaze icing

L. Gao · R. Veerakumar · Y. Liu · H. Hu (✉)
Department of Aerospace Engineering, Iowa State University, Ames, IA 50011-2271, USA
E-mail: huhui@iastate.edu

Published online: 25 May 2019

condition. During the experiment, while a high-speed imaging system was used to record the dynamic ice accretion process over the surfaces of the turbine blade model, a novel Digital Image Projection (DIP)-based 3D scanning system was also used to quantify the 3D shapes of the complex ice structures accreted over the test model. To the best knowledge of the authors, this is the first effort of its nature. The objective of the present study is to characterize the dynamic ice accretion process and to quantify the time evolution of the complex ice structures accreted over wind turbine blade surface for a better understanding of the wind turbine icing phenomena, which is essential for the development of effective and robust anti-/de-icing strategies tailored specifically for wind turbine icing mitigation.

2 Experiment setup and test model

The experimental study was performed in Icing Research Tunnel located at Iowa State University (i.e., ISU-IRT). As shown schematically in Fig. 1, ISU-IRT is a research-grade multifunctional icing tunnel with a transparent test section of 0.40 m × 0.40 m × 2.0 m in size. It can be used to simulate/duplicate a wide range of icing conditions from dry rime icing to extreme wet glaze icing by adjusting the wind speed (i.e., V_∞ = 5.0 ~ 60 m/s), ambient temperature (i.e., T_∞ = − 25 ~ 20 °C), the liquid water content level (i.e., LWC = 0.1 ~ 5.0 g/m^3) of the incoming airflow and the water droplet size in ISU-IRT. Further information about the technical details of ISU-IRT is available at Liu and Hu (2018). In the present study, a typical glaze icing condition that wind turbines usually experience in cold and wet winters (Lamraoui et al. 2015) was simulated with the controlling parameters of wind speed of V_∞ = 40 m/s (i.e., a typical wind speed at outer bound region of turbine blades), ambient temperature of T_∞ = − 5.0 °C and LWC = 1.1 g/m^3.

The wind turbine blade model used in the present study was designed based on DU91-W2-250 airfoil shape in the cross section. DU91-W2-250 airfoil, which is a cambered airfoil with a blunt leading edge and a maximum thickness of 25% chord length, is known for its favorable aerodynamic performance and strong structural strength for wind turbine applications. The test model used in the present study has a chord length (C) of 150 mm (i.e., C = 0.15 m) and spanwise length of 400 mm. It was 3D printed with a hard plastic

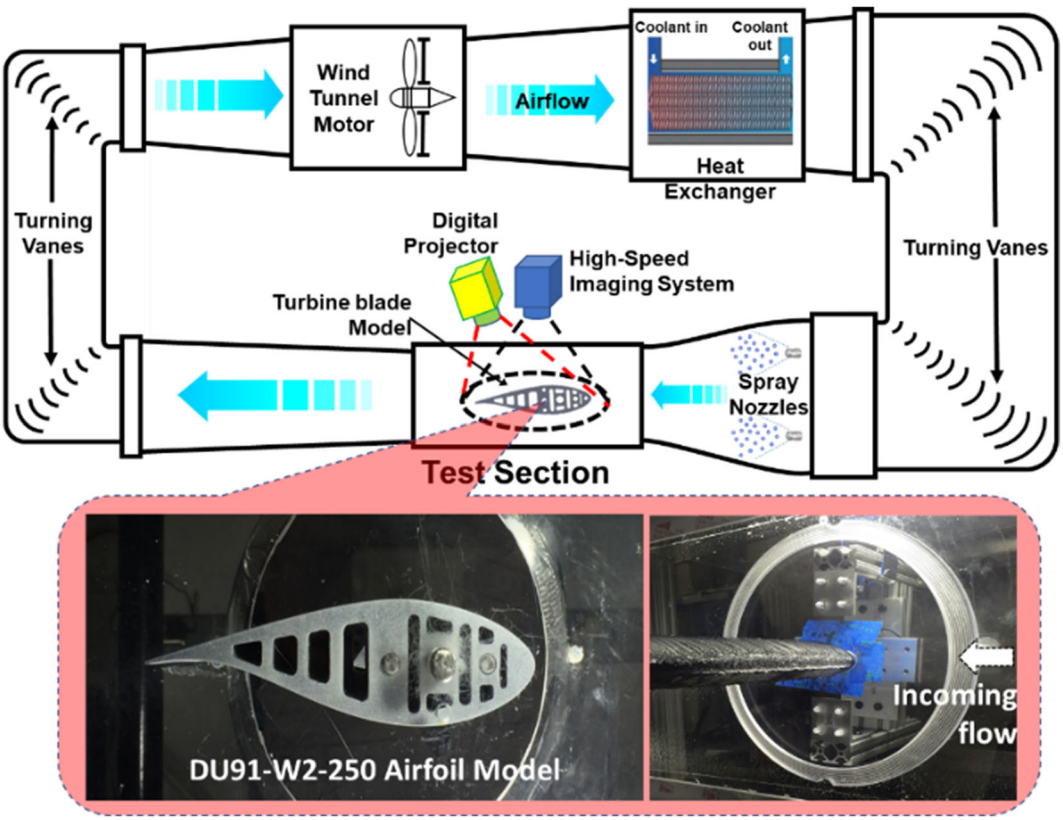

Fig. 1 Schematics of ISU-IRT and experimental setup used in the present study

material, VeroWhitePlus, which has a very similar physical properties (i.e., thermal conductivity k = 0.22 W/mK and density ρ = 1.28 kg/m^3) and surface wettability of the composite-based wind turbine blades (Senis et al. 2017). The surface of the test model was wet-sanded by using a series of progressively finer sandpapers (up to 2000 grit) to achieve a very smooth, glossy finish with a characteristic roughness of about 20 μm. During the ice accretion experiments, the test model is mounted in the middle of the ISU-IRT test section with an angle of attack of 10 deg.(i.e., AoA = 10 deg.), which is the most commonly used AoA for wind turbine operation, as described in Gao et al. (2019).

During the ice accretion experiments, a high-resolution imaging system (i.e., PCO Tech, Dimax Camera, 2 K pixels × 2 K pixels in spatial resolution) along with a 60-mm Macro Lens (Nikon, 60 mm Nikkor 2.8D) was used to record the dynamic ice accreting process over the surface of the turbine blade model. The camera was positioned normal to the airfoil chord of the test model. Low-flicker illumination was provided by a pair of 150 W fiber-coupled halogen lamps (AmScope, HL250-AS).

In addition to acquiring snapshot images to visualize the dynamic ice accretion process, a novel Digital Image Projection (DIP)-based 3D scanning system was also used to achieve "in situ" measurements of the 3D shapes of the ice structures accreted over the surface of turbine blade model. The DIP system is based on the principle of structured light triangulation in a fashion similar to stereo vision technique, but replacing one of the cameras in the stereo pair with a digital projector. A digital image with known pattern characteristics was projected onto the test object of interest (i.e., ice structures accreted over the surface of the turbine blade model for the present study). Due to the complex three-dimensional (3D) geometrical profiles of the test objects (i.e., the top surfaces of the accreted ice structures), the projected digital patterns are deformed when observed from a perspective different from the projection axis. By comparing the distorted digital patterns (i.e., acquired images with ice structures accreted over the surface of the turbine blade model) with a reference digital pattern without the test objects on the reference surface, the 3D profile of the test objects (i.e., the accreted ice structures over the surface of the test model) can be retrieved quantitatively. Further information about the technical basis and implementation of the DIP system is available in Zhang et al. (2015).

As shown schematically in Fig. 1, the DIP-based 3D scanning system was used to achieve "in situ" measurements of the 3D shapes of the ice structures with the iced test model still being mounted inside ISU-IRT. After conducting a careful calibration operation to register the correlation relationship between the digital projector and high-resolution camera, the iced test model was rotated at every 60 degrees around its pivot point (i.e., the aerodynamic center at 25% chord length of the airfoil model) for the DIP image acquisitions. The DIP images were processed to retrieve 3D profiles of the ice structures acquired at different phase angles and then combined automatically to reconstruct the 3D shapes of the ice structures accreted over both the upper and lower surfaces of the test model.

It should be noted that while a number of intrusive methods have been developed for quantitative measurements of ice shapes accreted over airfoil models, e.g., hand-tracing method (Lee et al. 2012), and mold and casting method (Blasco et al. 2017), they are usually very time-consuming and expensive in implementation (i.e., mold and casting method). Furthermore, some of the fragile ice features might even be damaged during the ice shape measurements. More recently, non-intrusive laser light-sheet scanning technique has also been developed for 3D ice shape measurements (Gong and Bansmer 2015; Woodard et al. 2018). However, the laser scanning method can only measure 2D profiles of accreted ice structures directly and relies on a line-by-line scanning operation to reconstruct 3D ice shapes, which could be quite time-consuming and much involved in instrumentation for high-resolution measurements of complex 3D ice structures. The DIP-based 3D scanning system used in the present study is a stereo-vision-based technique, which is capable of quantitatively measuring fully 3D shapes of complex ice structures accreted over the airfoil model. In comparison with those conventional methods (i.e., hand-tracing method, mold and casting method or laser light-sheet scanning technique), the DIP-based 3D scanning system is much faster (i.e., $\sim$ 10 s for each test case) to achieve full 3D shape measurements of ice structures over the entire span of the test model and also much easier to implement for "in situ" measurements of 3D ice shapes with the test model mounted in the icing tunnel. For the 3D scanning operation, while the airflow was paused, the ambient temperature was kept at the same level. The change in the morphology of the ice surface is believed to be very small due to the scanning operation. For the measurement results given in the present study, while the spatial resolution of the DIP measurements was about $\sim$ 0.50 mm, the uncertainty in the measured ice thickness was estimated to be $\sim$ 200 μm.

3 Experimental results and discussion

Figure 2 shows typical snapshot images acquired by using the high-speed imaging system to qualitatively reveal the dynamic ice accreting process over both the upper and lower surfaces of the turbine blade model as a function of the ice accretion time (i.e., after switching on the water spray system of ISU-IRT at the time instance of $t = t_0$). It can be seen clearly that upon the impacting of the supercooled water droplets carried by the incoming airflow, ice structures were found to accrete very rapidly on both the suction side (i.e., upper surface) and pressure side (i.e., lower surface) of the test model. Under the test condition of V_∞ = 40 m/s, T_∞ = − 5 °C and LWC = 1.1 g/m^3, the ice accretion process on the test model was found to be a typical glaze icing process with obvious surface water runback and formation of transparent, glassy ice structures, as described in Waldman and Hu (2015).

It can also be seen that with the test model was mounted at AoA = 10 deg., supercooled water droplets carried by the incoming airflow would impact mainly onto the pressure side of the airfoil surface, concentrating in the region near the airfoil leading edge. As a result, majority of the ice structures were found to accrete over the pressure-side surface of the test model, mainly in the region near the airfoil leading edge, as expected. As described in Liu and Hu (2018), due to the inadequate heat transfer to remove/dissipate all the released latent heat of fusion associated with the solidification process under such a wet glaze icing condition, only a portion of the supercooled water droplets would be frozen into ice instantly upon impacting onto the airfoil surface, while the remaining portion of the impacted water mass would stay in liquid phase. As driven by the aerodynamic shear force exerted by the boundary layer airflow over the airfoil surface, the unfrozen surface water accumulated near the airfoil leading edge would run back along the airfoil surface to form rivulet flows at further downstream, as that described in Zhang et al. (2015). The runback surface water was found to be frozen into ice eventually in the form of rivulet-shaped ice structures. While majority of ice accretions were found to occur over the pressure-side surface of the test model,

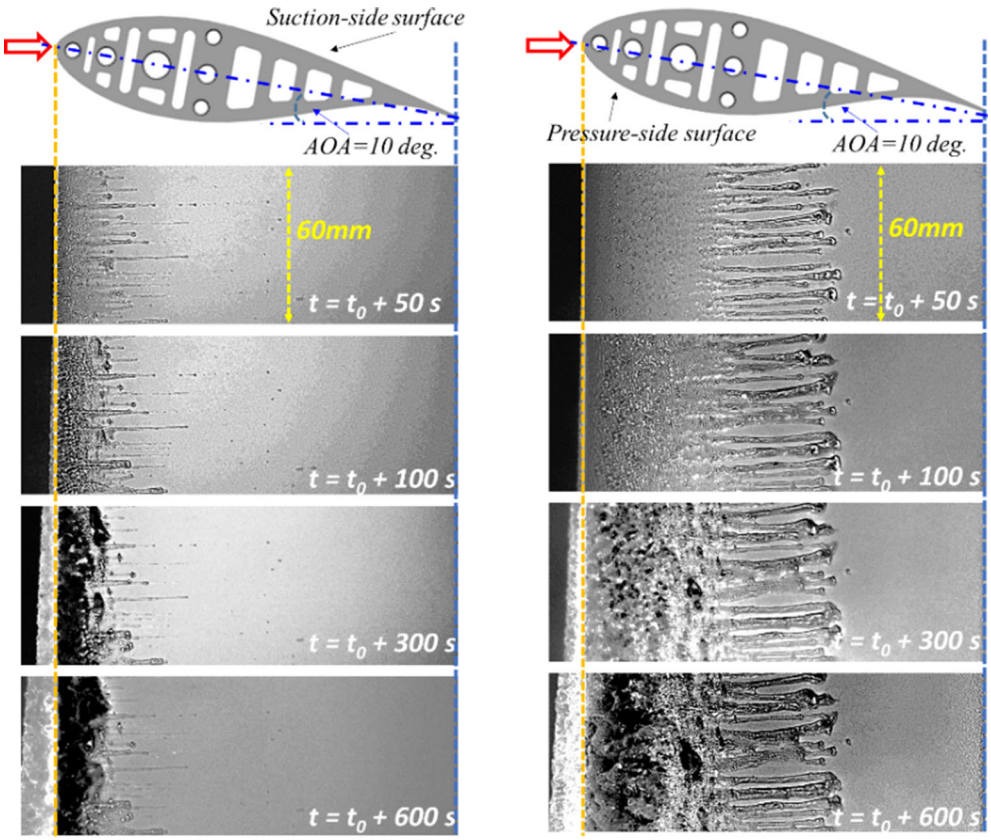

(a) over the suction-side surface **(b)** over the pressure-side surface

Fig. 2 Acquired snapshot images to qualitatively reveal the dynamic ice accreting process over the suction-side and pressure-side surfaces of the turbine blade model. **a** Over the suction-side surface and **b** over the pressure-side surface

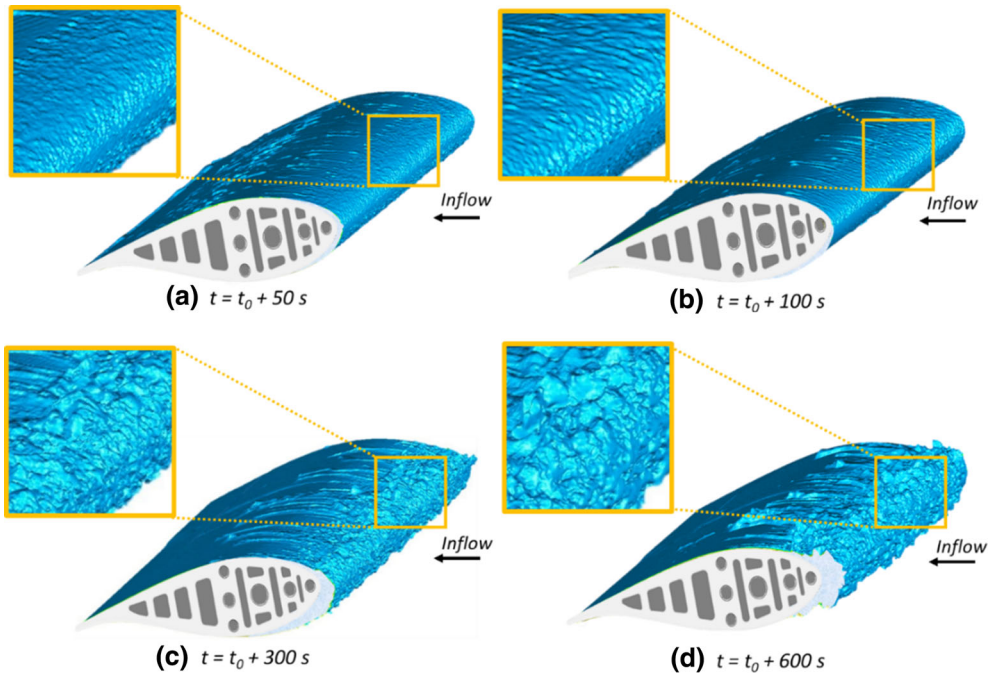

Fig. 3 Time evolution of the 3D shapes of the ice structures accreted over the surface of the turbine blade model under a typical glaze icing condition of V_∞ = 40 m/s, LWC = 1.1 g/m^3 and T_∞ = − 5.0 °C

irregular-shaped ice structures were also found to accrete over the suction-side surface of the test model, mainly near the airfoil leading edge. As the ice accretion time increases, with more and more supercooled water droplets impacting onto the test model, the ice layer accreted on the turbine blade model was found to become thicker and thicker, as shown clearly in Fig. 2.

Figure 3 gives the typical measurement results of the DIP-based 3D scanning system at four representative instants, i.e., at 50 s, 100 s, 300 s and 600 s, after starting the ice accretion experiment. The characteristics of the dynamic ice accreting process as well as time evolution of the complex ice structures accreted on the turbine blade model were revealed much more clearly and quantitatively from the measurement results. As shown clearly in Fig. 3, upon the impacting of the supercooled water droplets onto the airfoil surface, a thin layer of ice/water mixtures was found to form immediately over the surface of the test model, mainly near the airfoil leading edge (i.e., within the direct impinging zone of the supercooled water droplets). Since only a portion of the impacted supercooled water droplets would be frozen into ice instantly under such a wet glaze icing condition, the unfrozen impacted water mass was found to run back readily along the airfoil surface to form rivulet flows. The runback surface water was found to be frozen into ice eventually to form isolated rivulet-shaped ice structures at further downstream regions, i.e., in the downstream region far beyond the direct impacting zone of the supercooled water droplets. As revealed clearly in the "zoom-in" views of the ice accretion images, the surface of the iced test model was found to become rougher and rougher as the ice accretion time increases.

2D profiles of the accreted ice structures at different spanwise locations of the test model were extracted based on the 3D DIP measurements results in order to reveal the complex ice structures accreted over the surface of the turbine blade model more quantitatively. Figure 4 gives the 2D profiles of the accreted ice structures in five cross sections (i.e., sections S1–S5, which are evenly spaced over a 10-inch span in the middle portion of the test model) after 600 s of the ice accretion experiment. It can be seen clearly that the 2D ice shape profiles extracted at different cross sections were found to overlap with each other well in general, indicating the dominant 2D features of the ice accretion process over the 2D test model, as expected. However, obvious differences in the accreted ice shape at different spanwise locations (i.e., spanwise variations) can also be observed, especially in the region near the airfoil leading edge. The spanwise variations in the accreted ice shapes (e.g., formation of 3D-bulged ice structures and rivulet-shaped ice structures at further downstream location) are believed to be closely related to the wet nature of glaze

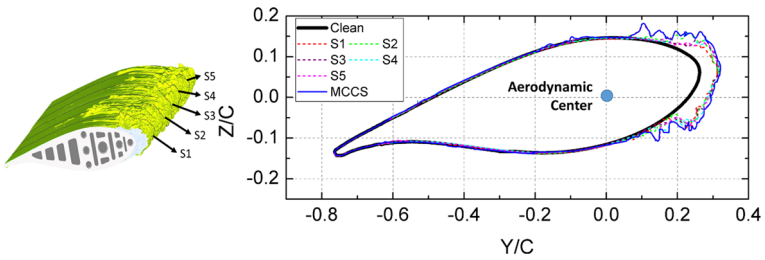

Fig. 4 2D profiles of the accreted ice structures at different spanwise sections and the resultant MCCS profile

icing process, caused by the complicated interplaying among multiphase flows (i.e., incoming airflow, impinging supercooled water droplets and runback surface water and ice accreting airfoil surface).

Following the work of Woodard et al. (2018), a concept of "maximum combined cross section" (MCCS) profile of the accreted ice structures is used in the present study to highlight the irregular features of the ice structures accreted on the turbine blade model. By projecting the section cuts of the accreted ice structures at different spanwise locations onto a single plane, the MCCS profile of the ice structures accreted over the test model is obtained by tracing the maximum outer boundary of the ice structures. As shown clearly in Fig. 4, the MCCS profile would represent the outermost extent of the ice structures accreted over the surface of the turbine blade model.

The MCCS profiles of the ice structures accreted on the turbine blade model at different time instants during the dynamic ice accretion process can also be obtained with the same procedure as that described above. Figure 5 shows the variations in the MCCS profiles of the accreted ice structures as a function of the ice accretion time, which can be used for validation and verification of various empirical and theoretical models for ice shape predictions. It can be seen clearly that at the earlier stage of the ice accretion experiments (i.e., $t \leq t_0 + 50$ s), the ice layer accreted over the surface of the test model was found to concentrate mainly in the region near the airfoil leading edge (i.e., within the direct impinging limit of the supercooled water droplets). The accreted ice layer was also found to conform well with the original profile of the "clean" airfoil surface with very small ice roughness over the iced airfoil surface. As the time goes by, with more and more supercooled water droplets impacting onto the iced airfoil surface, the ice layer accreted over the test model was found to become thicker and thicker. Corresponding to the runback of the unfrozen surface water under the wet glaze icing condition, while the coverage of the ice layer over the test model was found to extend to future downstream, the roughness of the iced airfoil surface was also found to increase rapidly. The much rougher surface of the iced turbine blade model, especially with the irregular-shaped ice structures accreted near the airfoil leading edge, would cause significant disturbances to the incoming airflow, which would result in large-scale flow separation over the airfoil surface, thereby, causing tremendous aerodynamic performance degradations to the wind turbine blades. As described in Gao et al. (2019), after the 600 s of the ice accretion experiment under the same glaze icing condition, the complex ice structures accreted over the turbine blade model would lead to the lift decrease to only about 30% of its original value, while the drag would increase about three times.

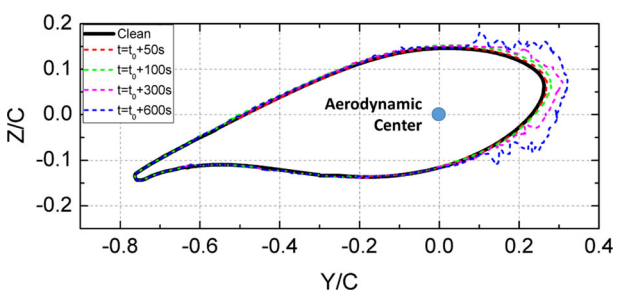

Fig. 5 Variations in the MCCS profiles of the ice accretion as a function of the ice accretion time

4 Conclusion

In summary, an experimental investigation was conducted to characterize the dynamic ice accretion process over the surface of a wind turbine blade model. The experimental study was performed in an Icing Research Tunnel available at Iowa State University (i.e., ISU-IRT). A turbine blade model with DU91-W2-250 airfoil shape in the cross section was manufactured and exposed to a typical wet glaze icing condition for the present study. During the experiment, in addition to using a high-speed imaging system to record the dynamic ice accretion process over the surfaces of the turbine blade model, a high-resolution Digital Image Projection (DIP)-based 3D scanning system was also used to quantify the 3D shapes of the ice structures accreted on the test model. The characteristics of the dynamic ice accretion process on the turbine blade model were revealed clearly and quantitatively in the term of the evolution of the 3D shapes of the ice structures accreted over the test model as a function of the ice accretion time. While the quantitative measurement data about the 3D shape changes in the ice structures accreted over the turbine blade model can be used for the validation and verification of various empirical and theoretical models for ice accretion predictions, the findings derived from the present study would also be very helpful to improve our understanding about the underlying icing physics pertinent to wind turbine icing phenomena, which is essential for the development of effective and robust anti-/de-icing strategies tailored specifically for wind turbines icing mitigation.

Acknowledgements This research is supported by National Science Foundation (NSF) under award numbers of OISE-1826978, CBET-1435590 and CMMI-1824840.

References

Battisti L (2015) Wind turbines cold climates: icing impacts and mitigation systems. Springer, Berlin. https://doi.org/10.1007/978-3-319-05191-8. ISBN 978-3-319-05190-1

Blasco P, Palacios J, Schmitz S (2017) Effect of icing roughness on wind turbine power production. Wind Energy 20:601–617. https://doi.org/10.1002/we.2026

Dalili N, Edrisy A, Carriveau R (2009) A review of surface engineering issues critical to wind turbine performance. Renew Sustain Energy Rev 13:428–438. https://doi.org/10.1016/j.rser.2007.11.009

Gao L, Liu Y, Zhou W, Hu H (2019) An experimental study on the aerodynamic performance degradation of a wind turbine blade model induced by ice accretion process. Renew Energy 133:663–675. https://doi.org/10.1016/J.RENENE.2018.10.032

Gong X, Bansmer S (2015) Laser scanning applied for ice shape measurements. Cold Reg Sci Technol 115:64–76. https://doi.org/10.1016/j.coldregions.2015.03.010

Hochart C, Fortin G, Perron J, Ilinca A (2008) Wind turbine performance under icing conditions. Wind Energy 11:319–333. https://doi.org/10.1002/we.258

Lamraoui F, Fortin G, Perron J, Benoit R (2015) Canadian icing envelopes near the surface and its impact on wind energy assessment. Cold Reg Sci Technol 120:76–88. https://doi.org/10.1016/j.coldregions.2015.09.007

Lee S, Broeren AP, Addy HE, et al (2012) Development of 3-D ice accretion measurement method. In: 4th AIAA atmospheric and space environments conference, pp 1–26. https://doi.org/10.2514/6.2012-2938

Li Y, Tagawa K, Feng F et al (2014) A wind tunnel experimental study of icing on wind turbine blade airfoil. Energy Convers Manag 85:591–595. https://doi.org/10.1016/j.enconman.2014.05.026

Liu Y, Hu H (2018) An experimental investigation on the unsteady heat transfer process over an ice accreting airfoil surface. Int J Heat Mass Transf 122:707–718. https://doi.org/10.1016/J.IJHEATMASSTRANSFER.2018.02.023

Morgan C, Bossany E, Seifert H (1998) Assessment of safety risks arising from wind turbine icing. In: Boreas VI—wind energy production in cold climate, pp 113–121

Senis E, Golosnoy I, Thomsen O et al (2017) Characterization of through-thickness thermal conductivity of wind turbine blade CFRP materials using a steady-state technique. In: 21st international conference on composite materials, Xi'an, China, 20–25 Aug 2017

Tammelin B, Cavaliere M, Holttinen H et al (1999) Wind energy production in cold climate (WECO). ETSU Contract Rep W/11/00452/REP, UK DTI 1–38

Waldman RM, Hu H (2015) High-speed imaging to quantify transient ice accretion process over an airfoil. J Aircr 53:369–377. https://doi.org/10.2514/1.C033367

Woodard BS, Broeren AP, Lee S et al (2018) Summary of ice shape geometric fidelity studies on an iced swept wing. Atmos Space Environ Conf 2018:1–41. https://doi.org/10.2514/6.2018-3494

Yin C, Zhang Z, Wang Z, Guo H (2016) Numerical simulation and experimental validation of ultrasonic de-icing system for wind turbine blade. Appl Acoust 114:19–26. https://doi.org/10.1016/j.apacoust.2016.07.004

Zhang K, Wei T, Hu H (2015) An experimental investigation on the surface water transport process over an airfoil by using a digital image projection technique. Exp Fluids 56:173. https://doi.org/10.1007/s00348-015-2046-z